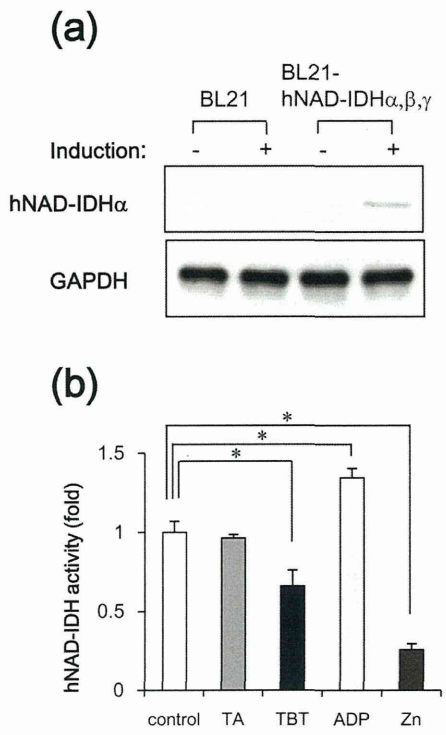

Figure 5 | Reduction of NAD-IDH enzyme activity by interaction with TBT in an E. coli expression system. (a) After the expression of pHIDHα, β, γ was induced by culturing E. coli BL21 transformants at 25°C for 20 h, crude extracts were prepared and were subjected to western blot analysis using the anti-NAD-IDHα and anti-GAPDH antibodies. Cropped blots were shown and the full-length blots were indicated in Supplementary Fig. 4. (b) After treatment with 100 nM TBT for 1 h, NAD-IDH activity was determined in the crude extracts. ADP (100 μM) and Zn^{2+} (2 mM) were used as positive and negative controls, respectively. * $P < 0.05$ compared with the corresponding control group.

TG-3′, reverse, 5′-GCACGACCTTGAGGGCAGCC-3′; rat NAD-IDHα: forward, 5′-TGGGTGTCCAAGGTCTCTC-3′, reverse, 5′-CTCCCACTGAATAGGTG-CTTTG-3′; rat NAD-IDHβ: forward, 5′-AGGCACAAGATGTGAGGGTG-3′, reverse, 5′-CAGCAGCCTTGAACACTTCC-3′; rat NAD-IDHγ: forward, 5′-TGGGCGGCATACAGTGACTA-3′, reverse, 5′-TTGGAGCTTACATGCAC-CTCT-3′; rat RPL13: forward, 5′-GGCTGAAGCCTACCAGAAAG-3′, reverse, 5′-CTTTGCCTTTTCCTTCCGTT-3′.

Aconitase activity assay. Aconitase activity was determined using the commercial Aconitase Activity Colorimetric Assay Kit (Biovision), according to the manufacturer's instructions. Briefly, NT2 cells were lysed in an assay buffer provided in the kit. The lysate was centrifuged at 14,000 g for 15 min, and the cleared supernatant was used for the aconitase assay.

NAD-IDHα knockdown experiment. Transient gene knockdown was performed using NAD-IDHα shRNA lentiviruses from Sigma-Aldrich (MISSION® shRNA) according to manufacturer's protocol. A scrambled hairpin sequence was used as a negative control. Briefly, the cells were infected with the viruses at a multiplicity of infection of 10, in the presence of 8 μg/ml hexadimethrine bromide (Sigma-Aldrich), for 24 h, and were then subjected to selection with 0.5 μg/ml puromycin for 72 h prior to functional analyses.

Tissue preparation. The present study was approved by the animal ethics committee and was conducted in accordance with the regulations on the use of living modified organisms of Hiroshima University. Male Slc:Wistar/ST rats (8 weeks old) were purchased from Japan SLC, Inc. (Shizuoka, Japan). They were housed under controlled temperature, 12 h light/dark cycle, and humidity (75 ± 5%) for at least 1 week prior to experiments. Standard pellet food and water were provided ad libitum. TBT solution (5 and 50 mg/kg body weight) was orally administered to rats. TBT was dissolved in polyethylene glycol. The whole brain was exposed by the use of fine scissors and forceps, and the frontal part of cerebral cortex was excised from the brain.

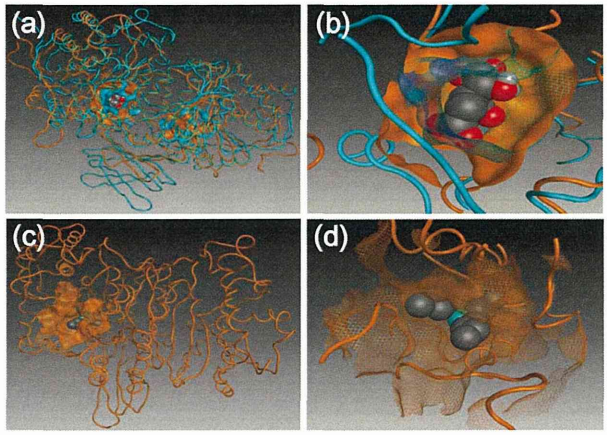

Figure 6 | *In silico* docking simulation analysis. (a) Overlaid structures of the calculated hNAD-IDHα (orange) and hNADP-IDH (cyan) homodimers bound to isocitric acid (Space-filling model). (b) The ligand binding pockets of the hNAD-IDHα (solid) and hNADP-IDH (wireframe) proteins. (c, d) Docking structure of hNAD-IDHα containing TBT (Space-filling model).

Transformation and Expression of Recombinant Human NAD-IDH Proteins in E. coli. pHIDHαβ1γ plasmid DNA (a kind gift from Dr. T. L. Huh) was used to transform E. coli BL21 (DE3) ultracompetent cells (BioDynamics, Tokyo, Japan). The colonies with positive inserts were subcultured and grown overnight at 37°C in LB medium (2 ml) supplemented with ampicillin (0.1 mg/ml). To express the enzyme, 15 ml tubes containing 2 ml of LB medium with 0.1 mg/ml ampicillin were inoculated with freshly grown E. coli cells (1% v/v), and these cultures were grown at 37°C while being shaken at 220 rpm for 4 h. The flasks were then temporarily placed in chilled water to lower the culture temperature to 25°C. Protein expression was induced in the cells by shaking at a lower speed of 140 rpm with minimal aeration at 25°C for 20 h. Then, 2 ml of the cell culture was centrifuged at 6,000 g for 15 min to separate the cells from the media, and the pellet was suspended in a total volume of 300 μl of cold assay buffer, a component of Isocitrate Dehydrogenase Activity Assay Kit. The suspended cells were subjected to 3 cycles of freeze-thaw before sonication (5 cycles of 15 sec sonication and 45 sec rest) and lysed. The cell lysate was centrifuged at 14,000 g for 15 min, and the cleared supernatant (crude extract) was separated. Recombinant human NAD-IDH activity was determined by subtracting basal activity in the crude extract from control BL21 cells.

Western blot analysis. Western blot analysis was performed as previously reported[34]. Briefly, the cells were lysed with Cell Lysis Buffer (Cell Signaling Technology, Danvers, MA, USA), and the proteins were separated by sodium dodecyl sulfate (SDS)-polyacrylamide gel electrophoresis and electrophoretically transferred to Immobilon-P (Millipore, Billerica, MA, USA). The membranes were probed with an anti-NAD-IDH (IDH3) α polyclonal antibody (1 : 1,000; Abcam, Cambridge, UK), an anti-β-actin monoclonal antibody (1 : 5,000; Sigma-Aldrich), and an anti-GAPDH monoclonal antibody (1 : 2,000; Abcam). The membranes were then incubated with secondary antibodies against rabbit or mouse IgG conjugated to horseradish peroxidase (Cell Signaling Technology). The bands were visualized using the ECL Western Blotting Analysis System (GE Healthcare, Buckinghamshire, UK), and the images were acquired using a LAS-3000 Imager (FUJIFILM UK Ltd., Systems, Bedford, UK). The density of each band was quantified using the ImageJ software (NIH, Bethesda, MD, USA).

In silico docking simulation studies. Homology modeling and docking studies of the human NAD-IDHα (hNAD-IDHα) and NADP-IDH (hNADP-IDH) homodimers were performed using Molecular Operating Environment (MOE) 2012.10. The models of hNAD-IDHα and hNADP-IDH were constructed based on the crystallographic structure of the porcine NADP-IDH homodimer (PDB: 1LWD)[35] using the standard protocols in MOE 2012.10. The docking simulations of the TBT-bound hNAD-IDHα and hNADP-IDH were carried out using ASEDock[36]. The TBT ligand was assigned in ASEDock, and the conformations were calculated using MMFF94S force field[37].

Statistical analysis. Results are shown as mean ± S.D. Statistical analysis was performed using one-way ANOVA followed by Dunnett's test. Differences at $P < 0.05$ were considered to be significant.

1. Toppari, J. *et al.* Male reproductive health and environmental xenooestrogens. *Environ. Health Perspect.* **104**, 741–803 (1996).

2. Hall, J. M. & Korach, K. S. Analysis of the molecular mechanisms of human estrogen receptors alpha and beta reveals differential specificity in target promoter regulation by xenoestrogens. *J. Biol. Chem.* **277**, 44455–44461 (2002).
3. Newbold, R. R., Padilla-Banks, E. & Jefferson, W. N. Adverse Effects of the Model Environmental Estrogen Diethylstilbestrol Are Transmitted to Subsequent Generations. *Endocrinology* **147**, s11–17 (2006).
4. Bulayeva, N. N., Gametchu, B. & Watson, C. S. Quantitative measurement of estrogen-induced ERK 1 and 2 activation via multiple membrane-initiated signaling pathways. *Steroids* **69**, 181–192 (2004).
5. Liu, D., Homan, L. L. & Dillon, J. S. Genistein acutely stimulates nitric oxide synthesis in vascular endothelial cells by a cyclic adenosine 5′-mono-phosphate-dependent mechanism. *Endocrinology* **145**, 5532–5539 (2004).
6. Watson, C. S., Alyea, R. A., Jeng, Y. J. & Kochukov, M. Y. Nongenomic actions of low concentration estrogens and xenoestrogens on multiple tissues. *Mol. Cell Endocrinol.* **274**, 1–7 (2007).
7. Bredfeldt, T. G. *et al.* Xenoestrogen-induced regulation of EZH2 and histone methylation via estrogen receptor signaling to PI3K/AKT. *Mol. Endocrinol.* **24**, 993–1006 (2010).
8. Gardlund, A. T. *et al.* Effects of prenatal exposure to tributyltin and trihexyltin on behavior in rats. *Neurotoxicol. Teratol.* **13**, 99–105 (1991).
9. Noda, T. *et al.* Teratogenicity study of tri-n-butyltin acetate in rats by oral administration. *Toxicol. Lett.* **55**, 109–115 (1991).
10. Whalen, M. M., Loganathan, B. G. & Kannan, K. Immunotoxicity of environmentally relevant concentrations of butyltins on human natural killer cells in vitro. *Environ Res.* **81**, 108–116 (1999).
11. Matthiessen, P. & Gibbs, P. E. Critical appraisal of the evidence for tributyltin mediated endocrine disruption in mollusks. *Environ. Toxicol. Chem.* **17**, 37–43 (1998).
12. McAllister, B. G. & Kime, D. E. Early life exposure to environmental levels of the aromatase inhibitor tributyltin causes masculinisation and irreversible sperm damage in zebrafish (Danio rerio). *Aquat. Toxicol.* **65**, 309–316 (2003).
13. Nishikawa, J. *et al.* Involvement of the retinoid X receptor in the development of imposex caused by organotins in gastropods. *Environ. Sci. Technol.* **38**, 6271–6276 (2004).
14. Kanayama, T., Kobayashi, N., Mamiya, S., Nakanishi, T. & Nishikawa, J. Organotin compounds promote adipocyte differentiation as agonists of the peroxisome proliferator-activated receptor gamma/retinoid X receptor pathway. *Mol. Pharmacol.* **67**, 766–774 (2005).
15. Grün, F. *et al.* Endocrine-disrupting organotin compounds are potent inducers of adipogenesis in vertebrates. *Mol. Endocrinol.* **20**, 2141–2155 (2006).
16. Cooke, G. M. Effect of organotins on human aromatase activity in vitro. *Toxicol. Lett.* **126**, 121–130 (2002).
17. Doering, D. D., Steckelbroeck, S., Doering, T. & Klingmüller, D. Effects of butyltins on human 5alpha-reductase type 1 and type 2 activity. *Steroids* **67**, 859–867 (2002).
18. McVey, M. J. & Cooke, G. M. Inhibition of rat testis microsomal 3beta-hydroxysteroid dehydrogenase activity by tributyltin. *J. Steroid Biochem. Mol. Biol.* **86**, 99–105 (2003).
19. von Ballmoos, C., Brunner, J. & Dimroth, P. The ion channel of F-ATP synthase is the target of toxic organotin compounds. *Proc. Natl. Acad. Sci. U S A* **101**, 11239–11244 (2004).
20. Yamada, S., Kotake, Y., Sekino, Y. & Kanda, Y. AMP-activated protein kinase-mediated glucose transport as a novel target of tributyltin in human embryonic carcinoma cells. *Metallomics* **5**, 484–491 (2013).
21. Vinekar, R., Verma, C. & Ghosh, I. Functional relevance of dynamic properties of Dimeric NADP-dependent Isocitrate Dehydrogenases. *BMC Bioinformatics* **13**, S2 (2012).
22. Birket, M. J. *et al.* A reduction in ATP demand and mitochondrial activity with neural differentiation of human embryonic stem cells. *J. Cell Sci.* **124**, 348–358 (2011).
23. Kim, Y. O. *et al.* Identification and functional characterization of a novel, tissue-specific NAD(+)-dependent isocitrate dehydrogenase β subunit isoform. *J. Biol. Chem.* **274**, 36866–36875 (1999).
24. Cohen, P. F. & Colman, R. F. Diphosphopyridine nucleotide dependent isocitratedehydrogenase from pig heart. Charactgerization of the active substrate and modes of regulation. *Biochemistry* **11**, 1501–1508 (1972).
25. Lemire, J., Mailloux, R. & Appanna, V. D. Zinc toxicity alters mitochondrial metabolism and leads to decreased ATP production in hepatocytes. *J. Appl. Toxicol.* **28**, 175–182 (2008).
26. Wise, D. R. *et al.* Hypoxia promotes isocitrate dehydrogenase-dependent carboxylation of α-ketoglutarate to citrate to support cell growth and viability. *Proc. Natl. Acad. Sci. U S A* **108**, 19611–19616 (2011).
27. Juang, H. H. Modulation of mitochondrial aconitase on the bioenergy of human prostate carcinoma cells. *Mol. Genet. Metab.* **81**, 244–252 (2004).
28. Gabriel, J. L., Zervos, P. R. & Plaut, G. W. Activity of purified NAD-specific isocitrate dehydrogenase at modulator and substrate concentrations approximating conditions in mitochondria. *Metabolism* **35**, 661–667 (1986).
29. Cho, S. A. *et al.* Up-regulation of Idh3alpha causes reduction of neuronal differentiation in PC12 cells. *BMB Rep.* **43**, 369–374 (2010).
30. Nakatsu, Y. *et al.* Glutamate excitotoxicity is involved in cell death caused by tributyltin in cultured rat cortical neurons. *Toxicol. Sci.* **89**, 235–242 (2006).
31. Atanasov, A. G., Nashev, L. G., Tam, S., Baker, M. E. & Odermatt, A. Organotins disrupt the 11beta-hydroxysteroid dehydrogenase type 2-dependent local inactivation of glucocorticoids. *Environ. Health Perspect.* **113**, 1600–1606 (2005).
32. le Maire, A. *et al.* Activation of RXR-PPAR heterodimers by organotin environmental endocrine disruptors. *EMBO Rep.* **10**, 367–373 (2009).
33. Kim, Y. O. *et al.* Characterization of a cDNA clone for human NAD(+)-specific isocitrate dehydrogenase alpha-subunit and structural comparison with its isoenzymes from different species. *Biochem. J.* **308**, 63–68 (1995).
34. Kanda, Y. & Watanabe, Y. Adrenaline increases glucose transport via a Rap1-p38MAPK pathway in rat vascular smooth muscle cells. *Br. J. Pharmacol.* **151**, 476–482 (2007).
35. Ceccarelli, C., Grodsky, N. B., Ariyaratne, N., Colman, R. F. & Bahnson, B. J. Crystal structure of porcine mitochondrial $NADP^+$-dependent isocitrate dehydrogenase complexed with Mn^{2+} and isocitrate. Insights into the enzyme mechanism. *J. Biol. Chem.* **277**, 43454–43462 (2002).
36. Goto, J., Kataoka, R., Muta, H. & Hirayama, N. ASEDock-docking based on alpha spheres and excluded volumes. *J. Chem. Inf. Model.* **48**, 583–590 (2008).
37. Halgren, T. A. MMFF VI. MMFF94s option for energy minimization studies. *J. Comput. Chem.* **20**, 720–729 (1999).

Acknowledgments

We thank Ms. Mami Kohno, Mr. Kyoichi Masuda, and Ms. Saki Tanaka (Graduate School of Biomedical and Health Sciences, Hiroshima University) for technical assistance in the animal experiment. This work was supported by a Grant-in-Aid for Scientific Research from the Ministry of Education, Culture, Sports, Science, and Technology, Japan (#23590322 to Y.K.), a Health and Labour Sciences Research Grant from the Ministry of Health, Labour and Welfare, Japan (Y.K.), and a grant from the Smoking Research Foundation (Y.K.).

Author contributions

S.Y. performed most of the experiments. Y.Ka. planned the project. S.Y., Y.S. and Y.Ka. wrote the manuscript. Y.Ko. performed the animal experiments. Y.D. and M.K. performed *In silico* docking simulation analysis. All authors reviewed the manuscript.

Additional information

Supplementary information accompanies this paper at http://www.nature.com/scientificreports

Competing financial interests: The authors declare no competing financial interests.

How to cite this article: Yamada, S. *et al.* NAD-dependent isocitrate dehydrogenase as a novel target of tributyltin in human embryonic carcinoma cells. *Sci. Rep.* **4**, 5952; DOI:10.1038/srep05952 (2014).

nature COMMUNICATIONS

ARTICLE

Received 28 Dec 2013 | Accepted 25 Jul 2014 | Published 25 Sep 2014

DOI: 10.1038/ncomms5806

Sphingosine-1-phosphate promotes expansion of cancer stem cells via S1PR3 by a ligand-independent Notch activation

Naoya Hirata[1], Shigeru Yamada[1], Takuji Shoda[2], Masaaki Kurihara[2], Yuko Sekino[1] & Yasunari Kanda[1]

Many tumours originate from cancer stem cells (CSCs), which is a small population of cells that display stem cell properties. However, the molecular mechanisms that regulate CSC frequency remain poorly understood. Here, using microarray screening in aldehyde dehydrogenase (ALDH)-positive CSC model, we identify a fundamental role for a lipid mediator sphingosine-1-phosphate (S1P) in CSC expansion. Stimulation with S1P enhances ALDH-positive CSCs via S1P receptor 3 (S1PR3) and subsequent Notch activation. CSCs overexpressing sphingosine kinase 1 (SphK1), an S1P-producing enzyme, show increased ability to develop tumours in nude mice, compared with parent cells or CSCs. Tumorigenicity of CSCs overexpressing SphK1 is inhibited by *S1PR3* knockdown or S1PR3 antagonist. Breast cancer patient-derived mammospheres contain SphK1$^+$/ALDH1$^+$ cells or S1PR3$^+$/ALDH1$^+$ cells. Our findings provide new insights into the lipid-mediated regulation of CSCs via Notch signalling, and rationale for targeting S1PR3 in cancer.

[1] Division of Pharmacology, National Institute of Health Sciences, Setagaya-ku, Tokyo 158-8501, Japan. [2] Division of Organic Chemistry, National Institute of Health Sciences, Setagaya-ku, Tokyo 158-8501, Japan. Correspondence and requests for materials should be addressed to Y.K. (email: kanda@nihs.go.jp).

Growing evidence suggests that many types of cancer, including breast, lung and prostate cancer, are initiated from a small population of cancer stem cells (CSCs; also called tumour-initiating cells)[1–8]. This minor population produces the bulk of cancers through continuous self-renewal and differentiation, which contributes to cancer heterogeneity. Therefore, it is essential to elucidate the signalling and regulatory mechanisms that are unique to CSCs, and to design novel therapeutic agents against CSCs.

CSCs have been isolated from diverse tumours and established cell lines, using several methods encompassing cell surface markers, aldehyde dehydrogenase (ALDH) activity, side population (SP) and sphere-forming ability. ALDH assays rely on the fact that the level of ALDH, a detoxifying enzyme responsible for the oxidation of intracellular aldehydes, is higher in stem cells than in differentiated cells[4]. ALDH1 expression is correlated with poor clinical prognosis in various cancers, such as breast, lung and prostate cancer[4–6]. Because CSCs have been considered to have molecular similarities to embryonic and normal adult stem cells, the self-renewal behaviour of CSCs has been reported to be mediated by several signalling pathways, such as Notch, Hedgehog and Wnt[9]. However, the molecular mechanisms that regulate the frequency and maintenance of CSCs via self-renewal signals remain poorly understood.

Autocrine and paracrine signalling plays a key role in maintaining the stem cell state and expansion of stem cells[10]. We therefore speculated that receptors for autocrine/paracrine factors might play a key role in CSC regulation. Using microarray screening in an ALDH-positive cell population of human breast cancer MCF-7 cells, we found that several receptors are upregulated. Among them, on the basis of pathophysiological properties, we focused on S1P receptor 3 (S1PR3), a receptor for a lipid mediator sphingosine-1-phospahate (S1P). S1P is known to exert multiple responses, such as proliferation, survival and cytoskeletal rearrangement, via its G protein-coupled receptor (GPCR) in many cell types[11]. S1P is synthesized from sphingosine by sphingosine kinase (SphK); two isoforms of mammalian SphK (sphingosine kinase 1 (SphK1) and SphK2) have been cloned and characterized[12,13]. In addition, the SphK1/S1P pathway has also been implicated in tumour progression[14,15]. S1P has also been shown to accumulate in the tumour microenvironment[16]. Although lipid mediators in cancer have been studied extensively, the role(s) of SphK1/S1P in CSCs remain unclear.

We demonstrate here that S1P regulates expansion of CSCs in several types of cancer. Our findings suggest that Notch activation is essential for S1P-induced proliferation of CSCs via S1PR3. We show that SphK1 regulates the tumorigenicity of breast CSCs via S1PR3. Using clinical samples, we show that breast cancer patient-derived CSCs contain SphK1$^+$/ALDH1$^+$ cells or S1PR3$^+$/ALDH1$^+$ cells. Thus, these results implicate the S1P signalling pathway as therapeutic targets in CSCs.

Results

S1P is a regulator of CSC population via S1PR3. We used an ALDH assay system to study the signalling pathways that regulate the frequency and maintenance of CSCs. Many cancer cell lines, including oestrogen receptor-positive MCF-7 cells, are known to contain an ALDH-positive cell population[5,6,17,18]. Consistent with a previous report[4], we confirmed that ALDH-positive cell population in MCF-7 cells possessed CSC-like properties, as assessed by expression of stem cell markers, drug resistance and tumorigenicity (Supplementary Fig. 1). Through microarray analysis, we investigated a possible receptor that increases the proportion of the ALDH-positive cell population in MCF-7 cells as a CSC model. We found *S1PR3* as a possible candidate in CSC regulation (Supplementary Data 1). *S1PR3* was highly expressed in the ALDH-positive cell population, a finding confirmed by quantitative polymerase chain reaction (qPCR) assays (Fig. 1a). *S1PR2* expression was lower in the ALDH-positive cell population compared with MCF-7 cells, and other types of *S1PR* are yet to be detected in MCF-7 cells (Supplementary Fig. 2)[19,20]. Stimulation with S1P increased the proportion of ALDH-positive cell population in a dose-dependent manner, with a maximal response observed at 100 nM (Fig. 1b). Similar to S1P, dihydro-S1P, another S1PR3 ligand, also increased the ALDH-positive cell population (Supplementary Fig. 3). Moreover, stimulation with S1P increased the number of SP cells (Fig. 1c), mammosphere-forming efficiency (Fig. 1d), CD44$^+$/CD24$^-$ population (Fig. 1e) and expression of stem cell markers (Fig. 1f). These data indicate that stimulation with S1P leads to an increase in breast CSCs. In contrast, lysophosphatidic acid (LPA), another well-studied lipid mediator, did not increase CSCs in MCF-7 cells. To confirm the involvement of S1PR3, we inhibited S1PR3 using pharmacological antagonists and RNA interference techniques. The effects of S1P were blocked by the S1PR3 antagonist TY52156 (ref. 21). Another antagonist CAY10444, which is structurally different from TY52156, also inhibited the S1P effect. In contrast, the S1PR2 antagonist JTE013 had little effect (Fig. 1g). Experiments using small interfering RNAs (siRNA) confirmed the effects of antagonists (Fig. 1h). In addition, short hairpin RNAs (shRNAs) against *S1PR3* also inhibited the enhancement of mammosphere-forming ability by S1P (Supplementary Fig.4). Similar results with ALDH assay were obtained in triple-negative MDA-MB-231 cells (Supplementary Fig. 5a,b), suggesting that S1P regulates both luminal and triple-negative type of breast CSCs. Furthermore, we examined CSCs from other tumour types to determine whether these effects of S1P are limited to breast cancer cell lines. Similar to MCF-7 cells, stimulation with S1P increased the ALDH-positive cell population in human lung cancer A549 cells, human prostate cancer LNCaP cells, human glioma U251MG cells and human ovarian cancer OVCAR-5 cells (Supplementary Fig. 6a). In addition, TY52156 inhibited the S1P effect in these cell lines. Taken together, these data demonstrate that S1P has an ability to increase the number of CSCs via S1PR3 in several types of cancer.

S1P enhances Notch signalling via S1PR3. Growing evidence suggests many similarities between embryonic stem cells and CSCs[9]; therefore, we focused on Notch, Hedgehog and Wnt as signalling pathway candidates downstream of the S1PR. Stimulation with S1P induced expression of the Notch target gene *Hes1* in MCF-7 cells (Fig. 2a) and ALDH-positive MCF-7 cells (Supplementary Fig. 7a). Moreover, S1P also induced the *Hes1* expression in ALDH-positive A549, LNCaP, U251 and OVCAR-5 cells (Supplementary Fig. 7b). S1P-induced *Hes1* expression was inhibited by S1PR3 antagonists (Fig. 2b). In contrast, the Hedgehog target gene *Gli1*, and Wnt target gene *Dkk1* were not induced. The effect of S1P on ALDH-positive cell population was inhibited by DAPT, an inhibitor of γ-secretase, which has multiple substrates including Notch, not by the Hedgehog inhibitor cyclopamine and the Wnt inhibitor PNU74654 (Fig. 2c; Supplementary Fig. 8). Similar effects of DAPT were obtained in MDA-MB-231 cells (Supplementary Fig. 5d), A549 cells, LNCaP cells, U251 cells and OVCAR-5 cells (Supplementary Fig. 6b). To determine whether S1P has the ability to activate the Notch pathway, we examined cleavage of Notch in MCF-7 cells. Stimulation with S1P produced the Notch intracellular domain (N1ICD) (Fig. 2d) and induced activation of the Notch transcriptional reporter *CSL*-luc (Fig. 2e). Because *Hes1* expression is dependent on NICD/CSL/MAML

complex-mediated gene transcription[22], we verified whether co-activators were involved in CSCs, using dominant-negative (DN) mutants of CSL, which have been reported to have no ability to bind to DNA[23]. DN-CSL inhibited S1P-induced *Hes1* expression and the ALDH-positive cell population (Fig. 2f). Similar results were obtained by DN-MAML, which lacks transcriptional activating domain and inhibits NICD-dependent transcriptional activition[24]. To examine which subtype of Notch was involved in CSCs, we overexpressed each type of NICD. Overexpression of N1ICD increased *Hes1* expression and the ALDH-positive cell population (Fig. 2g). N3ICD also increased the ALDH-positive cell population (Supplementary Fig. 9a), while N2ICD and

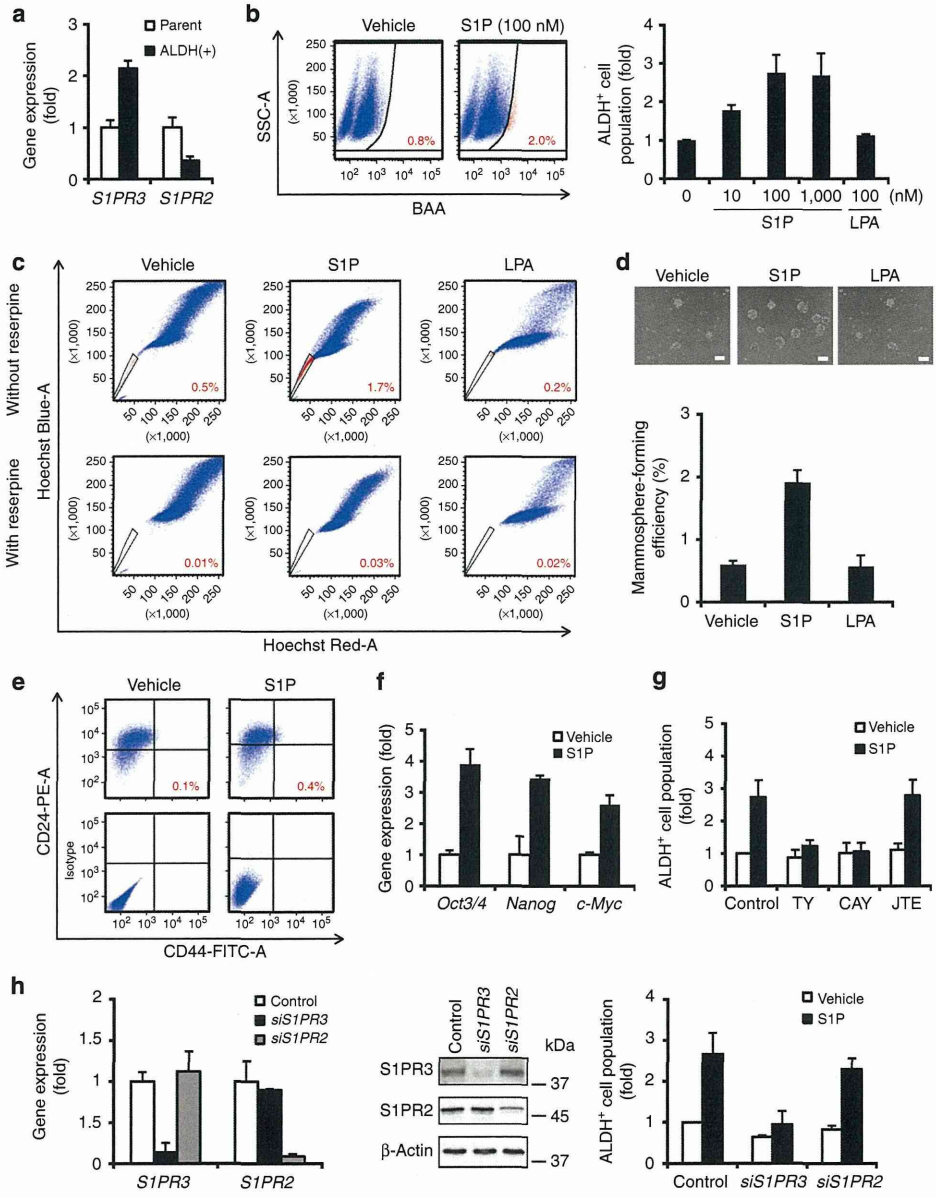

Figure 1 | Role of S1PR3 in the ALDH-positive cell population within the MCF-7 cell line. (**a**) Expression levels of S1PR (*S1PR2* and *S1PR3*) in parental or ALDH-positive MCF-7 cells by qPCR. Data represent mean ± s.d. ($n=3$). (**b**) Representative flow data with ALDH substrate in the presence or absence of S1P (100 nM, 3 days) in MCF-7 cells. Dose-dependent effects of S1P in the proportion of ALDH-positive cell population. Data represent mean ± s.d. ($n=3$). (**c**) Representative flow data of the SP assay with Hoechst 33342 dye alone or in the presence of reserpine (15 μg ml^{-1}). (**d**) Effects of S1P (100 nM) on mammosphere-forming efficiency in MCF-7 cells. The number of mammospheres was microscopically counted and the percentage of mammosphere-forming cells was determined as mammosphere-forming efficiency (%). The scale bar, 100 μm. Data represent mean ± s.d. ($n=3$). (**e**) Effects of S1P (100 nM) on CD44$^+$/CD24$^-$ population in MCF-7 cells. (**f**) Effects of S1P (100 nM) on expression of stem cell markers by qPCR. Data represent mean ± s.d. ($n=3$). (**g**) Effects of S1PR3 antagonists (TY52156, 1 μM; CAY10444, 10 μM) and the S1PR2 antagonist (JTE013, 10 μM) on S1P-induced increase in the ALDH-positive cell population. Data represent mean ± s.d. ($n=3$). (**h**) After transfection with siRNA, expression levels of S1P receptor were examined by qPCR and immunoblotting. Effects of siRNAs against *S1PR3* and *S1PR2* on S1P-induced increase in the ALDH-positive cell population. Data represent mean ± s.d. ($n=3$). Expression levels were normalized to glyceraldehyde 3-phosphate dehydrogenase messenger RNAs.

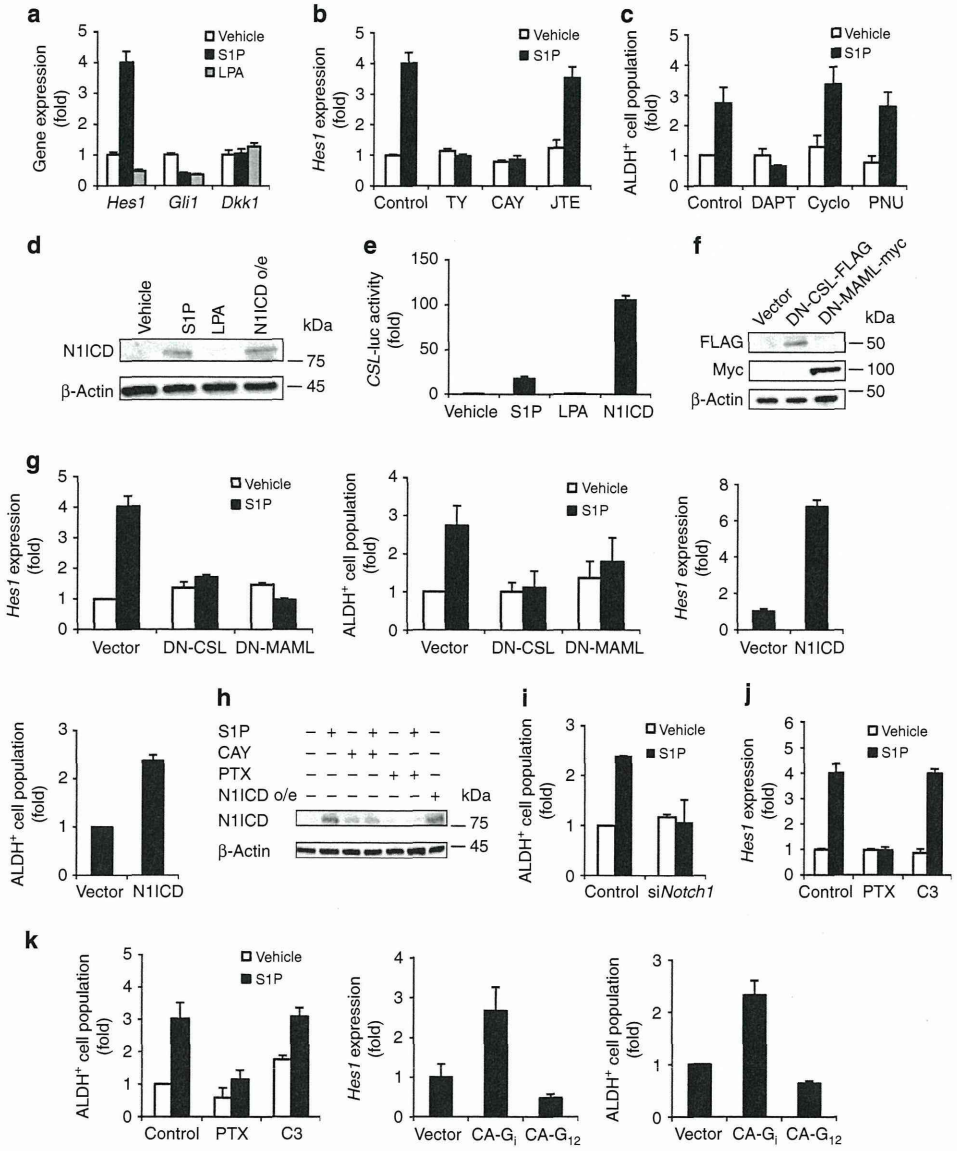

Figure 2 | Role of Notch signalling in ALDH-positive cell population. (**a**) After stimulation with S1P (100 nM) or LPA (100 nM) for 24 h, expression levels of the Notch target gene (*Hes1*), Hedgehog target gene (*Gli1*) and Wnt target gene (*Dkk1*) were quantified in MCF-7 cells using qPCR. Data represent mean ± s.d. ($n=3$). (**b**) Effects of TY52156 (1 μM) or CAY10444 (10 μM) on S1P-induced *Hes1* expression using qPCR. Data represent mean ± s.d. ($n=3$). (**c**) Effects of the Notch inhibitor DAPT (5 μM), the Hedgehog inhibitor cyclopamine (10 μM) or the Wnt inhibitor PNU74654 (10 μM) on S1P-induced increase in the ALDH-positive cell population. Data represent mean ± s.d. ($n=3$). (**d**) Effects of S1P or LPA on N1ICD production by immunoblotting. (**e**) MCF-7 cells transfected with a reporter plasmid encoding CSL-luc were cultured with or without S1P or LPA and were then analysed by luciferase assays. Data represent mean ± s.d. ($n=3$). (**f**) Effects of overexpression of Flag-tagged DN-CSL or myc-tagged DN-MAML on S1P-induced *Hes1* expression and ALDH-positive cell population. Data represent mean ± s.d. ($n=3$). The expression of plasmids was analysed by immunoblotting using tag-specific antibodies. (**g**) Effects of overexpression of N1ICD on *Hes1* expression and ALDH-positive cell population. Data represent mean ± s.d. ($n=3$). (**h**) After pretreatment with PTX (0.1 μg ml^{-1}, 24 h) or CAY10444 (10 μM, 30 min), the cells were stimulated with S1P. N1ICD production was analysed by immunoblotting with N1ICD-specific antibodies. (**i**) Effects of siRNA against *Notch1* on S1P-induced increase in the ALDH-positive cell population. Data represent mean ± s.d. ($n=3$). (**j**) Effects of toxins (PTX, 0.1 μg ml^{-1}; C3 Toxin, 0.1 μg ml^{-1}) on S1P-induced *Hes1* expression and ALDH-positive cell population. Data represent mean ± s.d. ($n=3$). (**k**) Effects of overexpression of CA mutants of G_i or G_{12} on S1P-induced *Hes1* expression and ALDH-positive cell population. Data represent mean ± s.d. ($n=3$). Expression levels were normalized to glyceraldehyde 3-phosphate dehydrogenase messenger RNAs.

N4ICD had little effect. S1P-induced N1ICD production was inhibited by CAY10444 (Fig. 2h); however, S1P did not induce N3ICD production (Supplementary Fig. 9b). To further examine the involvement of Notch in CSC, we performed knockdown experiments using *Notch1* siRNA. Knockdown of *Notch1* inhibited the effect of S1P on ALDH-positive cell population (Fig. 2i; Supplementary Fig. 10). Taken together, these data suggest crosstalk between S1P and Notch1. To confirm the

involvement of S1PR3 in crosstalk, we studied subtype of G proteins coupled to S1PR3. Pertussis toxin (PTX), which inactivates G_i protein, abolished S1P-induced *Hes1* expression and the ALDH-positive cell population, whereas C3 toxin, which inactivates an effector of $G_{12/13}$ Rho, had little effect (Fig. 2j). The effects of toxins were confirmed by overexpression of constitutively active (CA) mutants for G_i, but not by CA-G_{12} (Fig. 2k). These data suggest that G_i mediates S1P-induced Notch activation via S1PR3. Collectively, S1P has an ability to increase the number of CSCs via Notch signalling in several types of cancer.

S1P increases ADAM17 activity without Notch ligands. We further investigated the molecular mechanism of crosstalk between S1P and Notch in MCF-7 cells. Notch is generally activated by binding of Notch ligands to Notch and then cleaved by ADAM17 and γ-secretase[25]. Among Notch ligands (Jagged1, 2 and Delta-like ligand (Dll) 1, 3 and 4), Dll3 is not capable to activate Notch signalling in adjacent cells[26].

To examine whether Notch ligands are required for the S1P effect, we examined the expression level of Notch ligands. S1P did not induce expression levels of Notch ligands (Supplementary Fig. 11a). Knockdown of Notch ligands did not affect S1P-induced *Hes1* expression and ALDH-positive cell population (Fig. 3a,b). In contrast to S1P, knockdown of Notch ligands inhibited hypoxia-mimetic agent desferoxamine-induced *Hes1* expression. In addition, neutralizing antibodies to Jagged1 inhibited *Hes1* induction by soluble Jagged1-Fc, but not S1P-induced *Hes1* expression and ALDH-positive cell population (Supplementary Fig. 11c,d). Taken together, these data suggest that S1P activates Notch signalling in Notch ligand-independent manner.

We next studied cleavage enzymes that are responsible for S1P-induced Notch activation. We found that stimulation with S1P increased ADAM17 activity in MCF-7 cells (Fig. 3c) and ALDH-positive MCF-7 cells (Supplementary Fig. 7c). In addition, S1P also increased γ-secretase activity in MCF-7 cells (Supplementary Fig. 12a). CAY10444 and PTX inhibited S1P-induced ADAM17 activation (Fig. 3d) and γ-secretase activation (Supplementary Fig. 12b). Overexpression of CA-G_i also increased both ADAM17 (Fig. 3e) and γ-secretase activity (Supplementary Fig. 12c). Moreover, we examined whether ADAM17 activation occurred in CSCs. Overexpression of ADAM17 increased N1ICD production, *Hes1* expression and the ALDH-positive cell population (Fig. 3f). Conversely, DN-ADAM17 (E406A; point mutation at metalloprotease domain)[27] inhibited S1P-induced responses (Fig. 3g). Expression of ADAM10 or DN-ADAM10 (E384A; point mutation at metalloprotease domain)[28] had little effect on the CSC signalling pathway. These data suggest that ADAM17 is involved in S1P-induced CSC proliferation.

p38MAPK mediates ADAM17 activation by S1P. We investigated whether the intracellular domain of ADAM17 plays a role in S1P-induced breast CSC proliferation. ADAM17 activity is regulated by phosphorylation-dependent mechanisms[29–31]; therefore, we generated ADAM17 mutants with either Thr735 (p38MAPK consensus motif) or Thr761 (Akt consensus motif) replaced by alanine (Fig. 4a). Consistent with our data above, S1P induced ADAM17 phosphorylation at Thr735 (Fig. 4b). S1P-induced ADAM17 phosphorylation was inhibited by PTX and CAY10444. A mutation at Thr735 decreased ADAM17 phosphorylation through S1P, whereas a mutation at Thr761 had little effect (Fig. 4c). In addition, mutation of Thr735 inhibited S1P-induced ADAM17 activation, *Hes1* expression and the number of ALDH-positive cell population (Fig. 4d). To further confirm the involvement of p38MAPK, we studied the association between p38MAPK and ADAM17. Stimulation with S1P induced a transient phosphorylation of p38MAPK (Supplementary Fig. 13a) and an association between p38MAPK and ADAM17 (Fig. 4e). Mutation of Thr735 abolished this association (Fig. 4f), suggesting that phospho-p38MAPK binds to ADAM17 at Thr735. Treatment with CAY10444 or PTX also inhibited the S1P-induced association between p38MAPK and ADAM17 (Fig. 4g). The p38MAPK inhibitor SB203580 inhibited the S1P-induced responses (Supplementary Fig. 13b–d). Furthermore, SB203580 inhibited the association between p38MAPK and ADAM17 (Supplementary Fig. 13f). In contrast, the PI3-kinase/Akt pathway inhibitor LY294002 had little effect (Supplementary Fig. 13b–e). Taken together, these data suggest that p38MAPK-mediated ADAM17 activation is involved in the S1P-induced CSC phenotype.

SphK1 increases CSCs via S1PR3. S1P is synthesized through SphK-catalyzed phosphorylation of sphingosine[11,14]. We next examined whether SphK is involved in breast CSCs. Consistent with previous reports[32,33], overexpressed SphK1 was localized in the cytosol, and SphK2 was mainly localized to the nucleus (Fig. 5a). Enzyme activities of SphKs were also confirmed (Supplementary Fig. 14). Overexpression of SphK1 increased the number of ALDH-positive cell population in both MCF-7 (Fig. 5b) and MDA-MB-231 cells (Supplementary Fig. 15), whereas SphK2 had little effect. Consistent with the ALDH assay results, ADAM17 activation, N1ICD production and *Hes1* expression were induced by SphK1 but not SphK2 (Fig. 5c). To determine whether intracellular S1P is involved in the SphK1 effect, we tested the effects of the S1PR3 antagonist on SphK1-induced increases in the ALDH-positive cell population. Pretreatment with CAY10444 inhibited SphK1-induced responses (Fig. 5d). *S1PR3* shRNAs also inhibited these SphK1-induced responses (Fig. 5e). Analysis by qPCR confirmed specific suppression of *S1PR3* by these shRNAs (Fig. 5e), and treatment with PTX also produced similar results. Recent studies suggest that the ABC transporter mediates oestrogen-induced S1P secretion in MCF-7 cells[34]. To determine whether the ABC transporter is involved with the SphK1 effect, we used siRNAs and a selective inhibitor to inhibit the transporter. An siRNA against *ABCC1* inhibited SphK1-induced ADAM17 activation, *Hes1* expression and the ALDH-positive cell population (Supplementary Fig. 16a). The ABCC1 inhibitor MK571 also produced similar results (Supplementary Fig. 16b). In contrast, an siRNA against *Spns2*, another S1P transporter[35], had little effects. These data suggest that S1P produced by SphK1 stimulates S1PR3, and leads to an increase in the number of CSCs.

SphK1 accelerates tumour formation of CSCs via S1PR3. Since S1P is easily degraded by S1P lyase or phosphatases, we next studied tumorigenicity using SphK1- or SphK2-overexpressing CSCs in MCF-7 cells. Almost all nude mice injected with SphK1-overexpressing ALDH-positive cells developed tumours within 6 weeks. Tumour formation was inefficient in the mice injected with vector- or SphK2-overexpressing ALDH-positive cells (Fig. 6a,b). Tumour sizes from SphK1-overexpressing ALDH-positive cells were bigger than those from vector- or SphK2-overexpressing ALDH-positive cells (Fig. 6c,d). Histological analysis indicated that tumours derived from the ALDH-positive cells and the SphK1-overexpressing ALDH-positive cells had similar morphologies (Fig. 6e). To examine the proportion of ALDH-positive cells in xenografted tumour samples, we conducted double staining using ALDH assays and human-specific antibodies to TRA-1-85 (Supplementary Fig. 17). The increase in

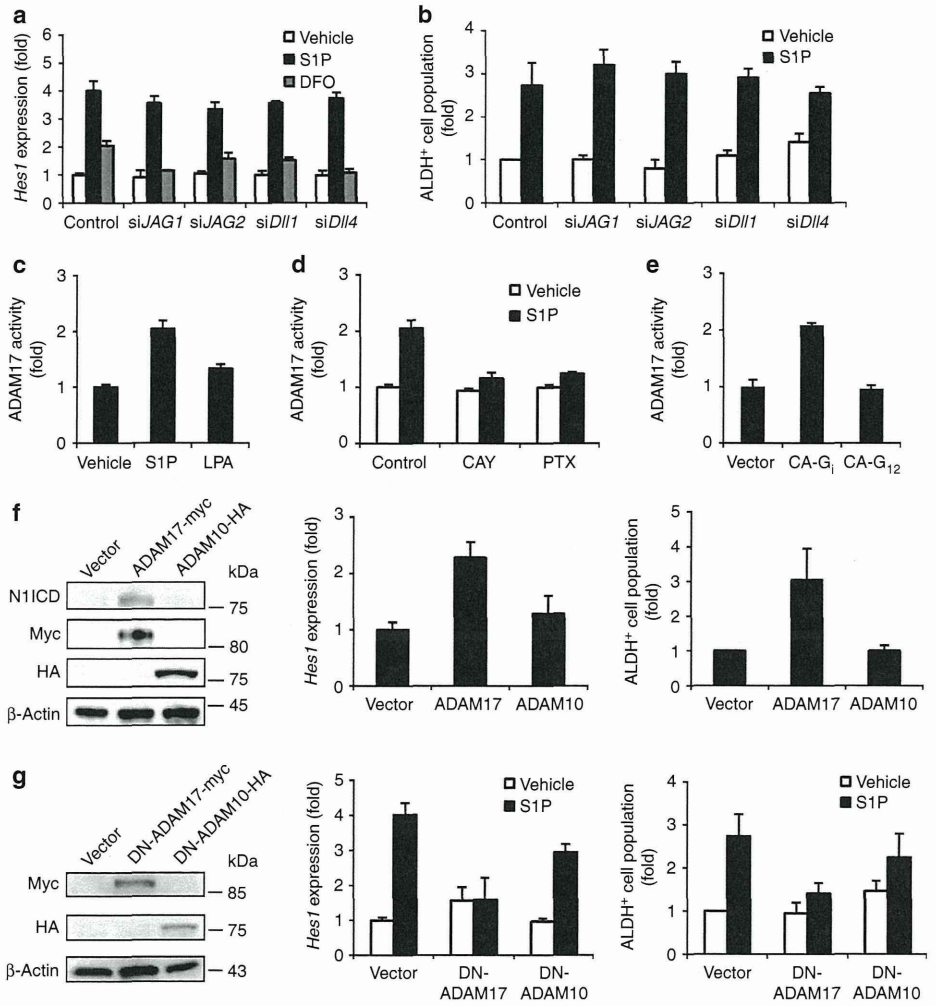

Figure 3 | S1P increases ALDH-positive cell population without Notch ligands. (**a**) Effects of siRNA against *Jagged1*, *Jagged2*, *Dll1* and *Dll4* on desferoxamine- or S1P-induced *Hes1* expression. Data represent mean ± s.d. ($n=3$). (**b**) Effects of siRNA against *Jagged1*, *Jagged2*, *Dll1* and *Dll4* on S1P-induced increase in ALDH-positive cell population. Data represent mean ± s.d. ($n=3$). (**c**) Stimulation with S1P (100 nM, 4 h) increased ADAM17 enzyme activity. Data represent mean ± s.d. ($n=3$). (**d**) S1P-induced ADAM17 activation was inhibited by CAY10444 (10 μM) and PTX (0.1 μg ml^{-1}). Data represent mean ± s.d. ($n=3$). (**e**) ADAM17 activation was induced by the overexpression of CA-G_{i}, but not by CA-G_{12}. Data represent mean ± s.d. ($n=3$). (**f**) Immunoblotting of N1ICD in ADAM17-myc- and ADAM10-HA-overexpressed MCF-7 cells. The expression of plasmids was confirmed using tag-specific antibody. Effects of overexpression of ADAM17 or ADAM10 on *Hes1* expression in MCF-7 cells. Effects of overexpression of ADAM17 or ADAM10 on ALDH-positive cell population in MCF-7 cells. Data represent mean ± s.d. ($n=3$). (**g**) Effects of DN mutants of ADAM17 or DN-ADAM10 on S1P-induced *Hes1* expression and the ALDH-positive cell population. Data represent mean ± s.d. ($n=3$). Expression levels were normalized to glyceraldehyde 3-phosphate dehydrogenase messenger RNAs.

the proportion of ALDH-positive cells in the tumour paralleled the *in vitro* results, suggesting a stem cell hierarchy (Fig. 6f). Histological analysis and double staining suggest that it is unlikely that the enhanced incidence of tumour formation by expression of SphK1 was due to cell differentiation. To examine whether S1PR3 and ALDH1 were co-expressed in the same cell, we performed double staining of ALDH1 and S1PR3 using xenografted tumour section (Supplementary Fig. 18). The number of ALDH1- and S1PR3 double-positive cells was increased in tumours derived from the SphK1-overexpressing ALDH-positive cells, compared with control and SphK2-overexpressing ALDH-positive cells. In addition, knockdown of *S1PR3* significantly inhibited the tumorigenicity of SphK1-overexpressing ALDH-positive cells, whereas knockdown of *S1PR2* had little effect (Fig. 6g). Furthermore, chronic administration of the S1PR3 antagonist TY52156 significantly inhibited the tumorigenicity of SphK1-overexpressing ALDH-positive cells (Fig. 6h). Taken together, both *in vitro* and *in vivo* results suggest that enhanced expression of SphK1 accelerated tumour formation of CSCs via S1PR3.

Patient-derived CSCs contain SphK1^{+}/ALDH1^{+} cells. We further extended our observations to primary cell culture. To examine *S1PR3* expression level in breast CSCs, we performed qPCR using secondary mammospheres from patient-derived tumour[8] (Supplementary Table 1). Similar to MCF-7 cells, *S1PR3* was highly expressed in ALDH-positive cells derived from breast cancer patient (Fig. 7a). In addition, we evaluated whether there

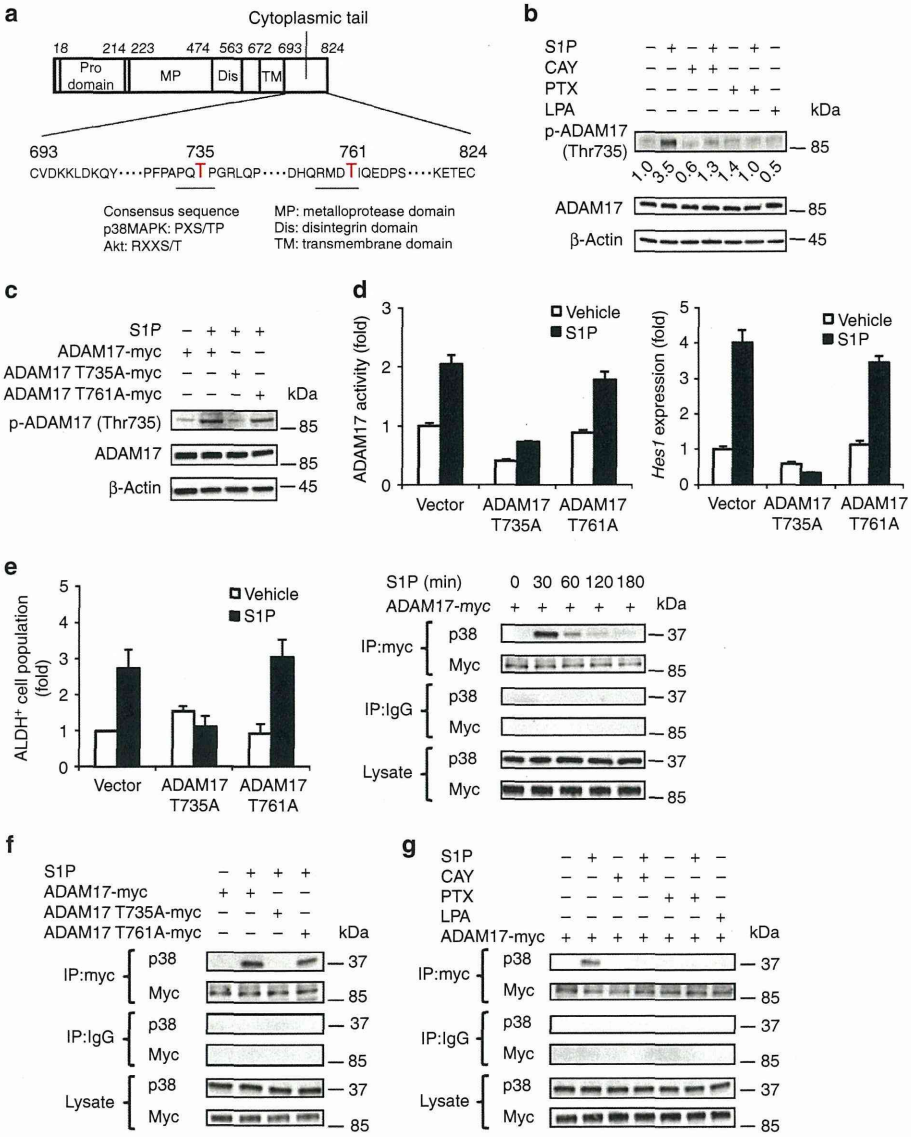

Figure 4 | S1P-induced ADAM17 activation via p38MAPK. (**a**) A schematic of the ADAM17 cytoplasmic domain mutants. (**b**) S1P-induced phosphorylation of ADAM17 at Thr735 was analysed by immunoblotting with a phospho-ADAM17 (Thr735)-specific antibody. (**c**) MCF-7 cells were transfected with ADAM17-T735A-myc or ADAM17-T761A-myc mutants and were then immunoblotted with phospho-ADAM17 (Thr735)-specific antibodies. (**d**) Effects of ADAM17-T735A and ADAM17-T761A mutants on S1P-induced ADAM17 activation, *Hes1* expression and ALDH-positive cell population. Expression levels were normalized to glyceraldehyde 3-phosphate dehydrogenase messenger RNAs. Data represent mean ± s.d. ($n=3$). (**e**) MCF-7 cells transfected with myc-tagged ADAM17 were either treated or untreated with S1P (100 nM) for the indicated times. The cells were then lysed and subjected immunoprecipitation with myc-specific antibodies, followed by p38MAPK-specific immunoblotting. (**f**) MCF-7 cells were transfected with myc-tagged ADAM17-T735A or T761A and stimulated with S1P (100 nM) for 30 min. The cells were then lysed and subjected to immunoprecipitation with myc-specific antibodies, followed by p38MAPK-specific immunoblotting. (**g**) MCF-7 cells transfected with myc-tagged ADAM17 were treated with S1P (100 nM) or LPA (100 nM) for 30 min in the presence or absence of CAY10444 (10 μM) or PTX (0.1 μg ml^{-1}). The cells were lysed and subjected to immunoprecipitation with myc-specific antibodies, followed by p38MAPK-specific immunoblotting.

were co-expressions of SphK1/ALDH1 or S1PR3/ALDH1 in breast CSCs by immunochemistry. Double staining demonstrated that these patient samples contained SphK1- and ALDH1 double-positive cells or S1PR3- and ALDH1 double-positive cells (Fig. 7b,c). We further evaluated whether SphK1, ADAM17 and N1ICD were co-expressed in the same cell. As a result, patient-derived tumour cells contained triple-positive cells (Fig. 7d). These data suggest that SphK1/S1PR3/Notch signalling is present in CSCs derived from breast cancer patient.

Discussion

In the present study, we used ALDH assays to identify regulators in CSCs, and determined that S1P/S1PR3 signalling and

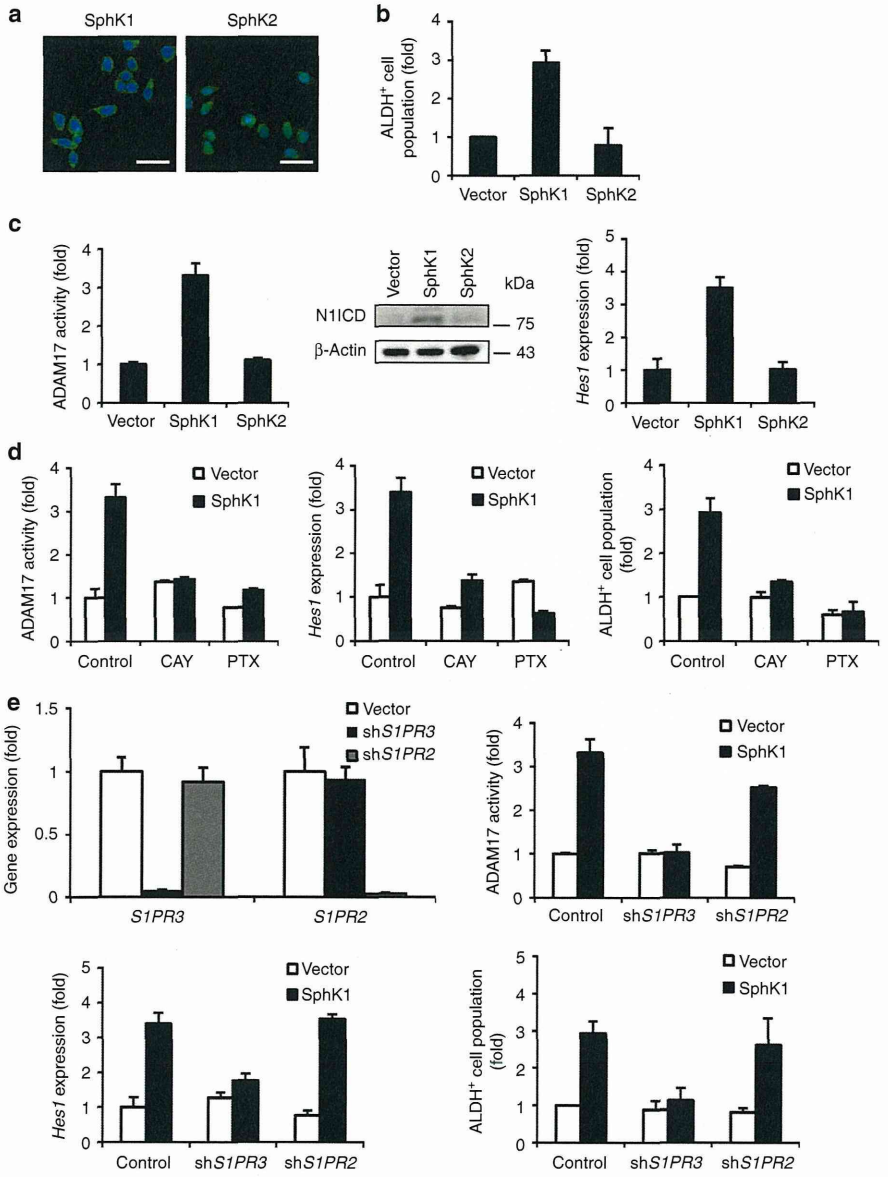

Figure 5 | Role of SphK1 in ALDH-positive cell population. (**a**) Expression of SphK in MCF-7 cells. Plasmid vectors encoding FLAG-tagged SphK1, or HA-tagged SphK2 were transfected into MCF-7 cells before SphK protein levels in cells were analysed by immunostaining. The scale bar indicates 20 μm. (**b**) Effects of SphK1 and SphK2 on the ALDH-positive cell population. Data represent mean ± s.d. ($n=3$). (**c**) Effects of SphK1 and SphK2 on ADAM17 activity, NICD production, and *Hes1* expression. Data represent mean ± s.d. ($n=3$). (**d**) Effects of CAY10444 (10 μM) and PTX (0.1 μg ml^{-1}) on the SphK1-induced ADAM17 activity, *Hes1* expression and ALDH-positive cell population. Data represent mean ± s.d. ($n=3$). (**e**) Expression level of S1P receptor in shRNA-transduced MCF-7 cells. Effects of shRNAs against *S1PR3* and *S1PR2* on the SphK1-induced ADAM17 activity, *Hes1* expression and ALDH-positive cell population. Data represent mean ± s.d. ($n=3$). Expression levels were normalized to glyceraldehyde 3-phosphate dehydrogenase messenger RNAs.

subsequent Notch activation resulted in an increase in the CSCs in several types of cancer (Fig. 8). S1PR3 antagonist inhibited the tumorigenicity of SphK1-overexpressed breast CSCs. Furthermore, breast cancer patient-derived CSCs contained SphK1$^+$/ALDH1$^+$ cells or S1PR3$^+$/ALDH1$^+$ cells. The findings presented here broaden our understanding of the role of lipids in CSC biology, and have significant clinical implications.

We found that S1P has the ability to induce proliferation of several types of CSCs, as stimulation with S1P activates Notch signalling, a key stem cell pathway. As such, S1P might have various roles in stem/progenitor cells. Indeed, S1P has been shown to maintain self-renewal of human embryonic stem cells in cooperation with platelet-derived growth factor[36]. Human-induced pluripotent stem cells have also been shown to express *S1PR3* messenger RNAs, although their biological effects in induced pluripotent stem cells are yet to be elucidated[37]. We postulate that S1P might have self-renewal properties, and play a key role in stem cell regulation.